AIMS Mathematics, 8(1): 295–316.
DOI: 10.3934/math.2023014
Received: 31 July 2022
Revised: 02 September 2022
Accepted: 06 September 2022
Published: 28 September 2022

http://www.aimspress.com/journal/Math

Research article

Significance of heat transfer for second-grade fuzzy hybrid nanofluid flow over a stretching/shrinking Riga wedge

Imran Siddique[1], Yasir Khan[2,*], Muhammad Nadeem[1], Jan Awrejcewicz[3] and Muhammad Bilal[4]

[1] Department of Mathematics, University of Management and Technology, Lahore 54770, Pakistan
[2] Department of Mathematics, University of Hafr Al Batin, Hafr Al Batin 31991, Saudi Arabia
[3] Department of Automation, Biomechanics and Mechatronics, Lodz University of Technology, 1/15 Stefanowskiego St., 90924 Lodz, Poland
[4] Department of Mathematics, The University of Chenab, Gujrat 50700, Pakistan

* **Correspondence:** Email: yasirkhan@uhb.edu.sa.

Abstract: This investigation presents the fuzzy nanoparticle volume fraction on heat transfer of second-grade hybrid Al_2O_3+Cu/EO nanofluid over a stretching/shrinking Riga wedge under the contribution of heat source, stagnation point, and nonlinear thermal radiation. Also, this inquiry includes flow simulations using modified Hartmann number, boundary wall slip and heat convective boundary condition. Engine oil is used as the host fluid and two distinct nanomaterials (Cu and Al_2O_3) are used as nanoparticles. The associated nonlinear governing PDEs are intended to be reduced into ODEs using suitable transformations. After that `bvp4c,' a MATLAB technique is used to compute the solution of said problem. For validation, the current findings are consistent with those previously published. The temperature of the hybrid nanofluid rises significantly more quickly than the temperature of the second-grade fluid, for larger values of the wedge angle parameter, the volume percentage of nanomaterials. For improvements to the wedge angle and Hartmann parameter, the skin friction factor improves. Also, for the comparison of nanofluids and hybrid nanofluids through membership function (MF), the nanoparticle volume fraction is taken as a triangular fuzzy number (TFN) in this work. Membership function and σ-cut are controlled TFN which ranges from 0 to 1. According to the fuzzy analysis, the hybrid nanofluid gives a more heat transfer rate as compared to nanofluids. Heat transfer and boundary layer flow at wedges have recently received a lot of attention due to several metallurgical and engineering physical applications such as continuous casting, metal extrusion, wire drawing, plastic, hot rolling, crystal growing, fibreglass and paper manufacturing.

Keywords: hybrid nanofluid; second-grade fluid; stagnation point flow; stretching/shrinking Riga wedge; TFN
Mathematics Subject Classification: 35Q30, 74F10, 76A05

1. Introduction

Interest in non-Newtonian fluid flows has expanded dramatically in recent decades due to its widespread use in food, chemical process industries, construction engineering, power engineering, petroleum production, and commercial applications. Furthermore, the boundary layer flow of non-Newtonian fluids is particularly important because of its application to a variety of engineering challenges, including the prospect of reducing frictional drag on ships and submarine hulls. Non-Newtonian fluids research gives engineers, mathematicians, and computer scientists some interesting and challenging challenges for these reasons. Non-Newtonian fluids include materials like ketchup, blood, silly putty, paints, suspensions, toothpaste and lubricants. Because shear rate and shear stress are nonlinearly associated in non-Newtonian fluids, perfect forecasting of all connected features for such fluids is not feasible using a single model. The classic Navier-Stock equation is useful for describing a variety of dynamics and rheological features of these fluids, including retardation, stress differences, memory effects, elongation, relaxation, yield stress, and so on. The class of viscoelastic/second-grade fluids is one category of differential type fluid for which analytic solutions can be reasonably expected. The viscoelasticity of fluids causes the order of differential equations describing the flow to grow. The normal stress effects can also be predicted using a second-grade fluid model. In their article, Rasool et al. [1] demonstrated the flow of second-grade fluid across an upright Riga surface. Abbas et al. [2] presented an entropy analysis of nanofluidic flow over a Riga plate. Shtern and Tsinober [3] investigated the stability of Blasius-type flow over a Riga surface. The mass and heat transfer of tangent hyperbolic nanofluids through a Riga wedge was inspected by Abdal et al. [4]. Over a Riga Plate, Gangadhar et al. [5] evaluated EMHD (Electro-magneto-hydro-dynamic) and Convective heat second-grade nanofluid. Khan and Alzahrani [6] evaluated the melting process and bioconvection on second-grade nanofluid through a wedge. In recent years, there has been a lot of study on second-grade liquid [7–13].

Several studies have shown that nanofluids have higher heat transfer capabilities than traditional fluids, which is why conventional fluids can be replaced with nanofluids. Nanotechnology has grown in relevance in different disciplines of science and the industrial zoon in recent years, making it one of the most powerful study areas. Researchers are paying particular attention to the varied thermal properties of such nano-sized nanoparticles because of the importance of nanoparticles in the generation of thermal engineering, multidisciplinary sciences and industries. The interaction of nanoparticles is being used in recent nanotechnology developments to improve the thermal transfer mechanism to meet the growing demand for energy resources. Nanoparticles' diverse uses in biomedical sciences include many illness diagnoses, heart surgery, cancer cell extinction, brain tumours, and a variety of medical applications. Thermally enhanced nanoparticles are used in numerous industrial applications such as heat and cooling processes, thermal extrusion systems, power generation and solar systems. Nanofluids are created by adding a small number of solid particles (10–100 nm range) [13]. Hybrid nanofluids are very useful for a variety of applications such as automobile radiators, biomedical, nuclear system cooling, coolant machining, microelectronic cooling, drug reduction, thermal storage and solar heating. On a mechanical level, they have

advantages like chemical stability and excellent thermal efficiency, allowing them to perform more efficiently than nanofluids. Suresh et al. [14] proposed the concept of hybrid terms. The hybrid nanofluid's experimental outcomes were also investigated. He demonstrated that hybrid nanofluids increased the heat transfer rate by two times more than nanofluids. Sundar et al. [15] examined the viscous fluid of a hybrid nanofluid at low volume fractions. The stagnation-point flow of hybrid nanostructured materials fluid flow was evaluated by Nadeem et al. [16]. The hybrid nanoparticle fluid flow in a cylinder was addressed by Nadeem and Abbas [17] with the slip effect. Yan et al. [18] inspected the rheological behaviour of a non-Newtonian hybrid nanofluid in the context of a driven pump. The viscosity of the hybrid nanofluid with the largest volume percentage was lowered by up to 21%, according to this study. Rahman et al. [19] used a moving edge to investigate the effects of internal heating, SWNCT and MWNCT on engine oil numerically. Aladdin et al. [20] proposed a hybrid nanofluid $Cu + Al_2O_3/H_2O$ flow above a moving permeable sheet. Several researchers are studying the heat transmission of hybrid nanofluids under various physical norms, as stated in [21–34].

In previous decades, fluids having higher electrical capacitance, such as fluid metals, were preferred. Externally applied (connected or common) magnetic disciplines of moderate strength can control the composition of the boundary layer in those types of liquids. The current created by the external field is insufficient to control the stream if the electrical permeability of the liquid (ocean water) is low, necessitating the use of an electromagnetic actuator to control it. Gailitis and Lielausis [35] invented that the Riga plate is unique in that it contains and imposes electric and magnetic fields strong enough to induce Lorentz forces parallel to the surface, thus restricting the flow of moderately conducting liquid. Also, the Riga-plate is a type of actuator. It could be utilized to prevent flow separation within an effective agent's radiation, skin friction, and subsurface pressure gradients. Basha et al. [36] investigated the stability of a hybrid $(Ag\text{-}MgO/H_2O)$ nanofluid flow over a stretching/shrinking Riga wedge with a stagnation point. Rasool and Wakif [37] used a modified Buongiorno's model to study numerically EHMD free convection of second-grade nanofluid on a vertical Riga plate. The EHMD flow of Maxwell nanofluid on the Riga plate was numerically explored by Ramesh et al. [38]. Shafiq et al. [39] evaluated the Marangoni impact across a Riga plate in the presence of CNTs. Ahmed et al. [40] examine the impact of thermal radiation and viscous dissipation on CNTs/water nanofluid over a Riga plate. Nanofluid with EMHD slip characteristics is analytically computed by Ayub et al. [41] using parallel Riga plates. The Riga plate was used by Zaib et al. [42] to consider the slip effect and mixed convective hybrid nanofluid flow. Abbas et al. [43] inspected entropy generation through a Riga plate. Bhatti et al. [44] numerically explained the viscous nanofluid across a Riga plate. Furthermore, numerous authors recently studied their work mentioned by [45–55] based on Riga plate flow.

Differential equations (DEs) play a very important role in explaining the framework for modelling systems in biology, engineering, physics and other disciplines. On the other side, when a real-world situation is simulated using ODEs, we can't always be sure that the model is working properly since dynamical framework information is sometimes inadequate or confusing. Authors employed a fuzzy environment instead of a fixed value to overcome this type of issue, transforming ODEs into fuzzy differential equations (FDEs). Zadeh [56] established the concept of fuzzy set theory (FST) in 1965. The FST was formulated to overcome uncertainty caused by a lack of information in many mathematical models. This theory has recently been investigated further with a variety of applications being explored. Chang and Zadeh [57] were the first to establish the concept of fuzzy derivatives. After that, Dubois and Prade [58] invented the extension principle. The fuzzy initial value problem was developed by Kaleva and Seikkala in [59–61]. In the last decades, researchers used

FDEs in fluid dynamics such as Borah et al. [62] used fractional derivatives to study the magnetic flow of second-grade fluid in a fuzzy environment. Later, Barhoi et al. [63] studied a permeable shrinking sheet in a fuzzy environment. Nadeem et al. [64] studied heat transfer analysis using fuzzy volume fraction. Additional information on FDEs and their applications are also offered in [65–73].

In the above literature, most of the researchers investigated the flow of different fluid models (Cassan, Maxwell and Newtonian fluid) over the wedge along with different physical impacts. Yet the flow of a second-grade fuzzy hybrid nanofluid past the wedge is not studied. Being inspired by the major features of a magnetic field, boundary slip, stagnation point flow, and heat transfer, the second-grade fuzzy hybrid nanofluid over a stretching/shrinking Riga wedge has been examined in the current study. The following points illustrate the novelty of this article:

- The use of aluminia $\left(Al_2O_3\right)$ and copper $\left(Cu\right)$ nanoparticles with engine oil (EO) as base fluid is considered.
- Thermal radiation is considered in nonlinear form.
- The volume fraction of Al_2O_3 and Cu nanoparticles is taken as a triangular fuzzy number.
- Thermal characteristics of nanofluids $\left(Al_2O_3/EO\right), \left(Cu/EO\right),$ and hybrid $\left(Al_2O_3+Cu/EO\right)$ nanofluids are compared with the help of the fuzzy membership function.

The subsequent research questions will be addressed as part of the appraisal of this study:

- What are the advantages of employing convective boundary conditions in the cooling process rather than a constant wall temperature?
- What effect would have second-grade fluid parameter have on the velocity profile?
- What will be the effect of nonlinear thermal radiation on thermal profile?
- What will be the impact of wedge angle on heat transfer rate?

2. Mathematical formulation

We suppose that an electrically conductive second-grade hybrid nanofluid flows incompressible past a stretching/shrinking Riga wedge with slip boundary conditions as shown in Figure 1. We have chosen aluminium $\left(Al_2O_3\right)$ and copper $\left(Cu\right)$ as nanoparticles with Engine oil (EO) as the base fluid. By examining the heat source, stagnation point, nano-linear thermal radiation, and convective boundary conditions. $u_{sv} = U_{sv}x^m$ is the free stream velocity and U_{sv} is a positive constant. The boundary wall is supposed to be moving, and a velocity slip is allowed, which is expressed on the wall as $u = u_v + Ru_y\left(0\right)$. Here, $u_v = U_v x^m$ indicates the wedge's stretched/shrunk velocity, with $U_v > 0$ identifying the stretching wedge, $U_v < 0$ representing the shrinking wedge, and $U_v = 0$ expressing the static wedge, and R signifies the slip coefficient. Further, $m = \psi/\left(2-\psi\right),$ where m is the Hartree pressure gradient, wedge angle is $\psi,$ and $\Gamma = \psi\pi$ defines the total angle of the wedge. Furthermore, it is important to note that the value of m is between 0 and 1, for stagnation point flow $\left(\Gamma = \pi\right)$ if $m = 1$ $\left(\psi = 1\right)$, the flow past a horizontal flat surface $\left(\Gamma = 0\right)$ if $m = 0$ $\left(\psi = 0\right)$. In this study, we consider the wedge flow problem so that the value of m must be in the

range of $0 < m < 1$. Also, $T_f > T_\infty$, where T_f is the surface temperature and T_∞ is the ambient temperature. The basic equations for hybrid nanofluid flow are given by [11,12,36,50] main assumption stated above.

$$\frac{\partial v}{\partial y} + \frac{\partial u}{\partial x} = 0, \tag{1}$$

$$u\frac{\partial u}{\partial x} + v\frac{\partial u}{\partial y} = \frac{\mu_{hnf}}{\rho_{hnf}}\frac{\partial^2 u}{\partial y^2} + \frac{\alpha_1}{\rho_{hnf}}\left(\frac{\partial u}{\partial x}\frac{\partial^2 u}{\partial y^2} + \frac{\partial^3 u}{\partial x \partial y^2} - \frac{\partial u}{\partial y}\frac{\partial^2 v}{\partial y^2} + v\frac{\partial^3 u}{\partial y^3}\right) + u_{sv}\frac{\partial u_{sv}}{\partial x} + \rho_f \frac{\pi j_0 M_0}{8\rho_{hnf}} e^{-\pi y/d}, \tag{2}$$

$$u\frac{\partial T}{\partial x} + v\frac{\partial T}{\partial y} = \frac{k_{hnf}}{(\rho c_P)_{hnf}}\frac{\partial^2 T}{\partial y^2} + \frac{16\delta^* T_\infty^3}{3k^*(\rho c_P)_{hnf}}\frac{\partial^2 T}{\partial y^2} + \frac{(T - T_\infty)}{(\rho c_P)_{hnf}} Q_0, \tag{3}$$

the boundary conditions are:

$$\begin{aligned} &v(x,0) = v_w, \ u(x,0) = u_w + \mu_{hnf}\frac{\partial u}{\partial y}, \ -k_{hnf}\frac{\partial T}{\partial y} = h_f(T - T_w), \ \text{at } y \to 0, \\ &u \to u_{sv}, \ T \to T_\infty, \ \text{at } y \to \infty. \end{aligned} \tag{4}$$

The velocities in the y and x directions are represented by v and u, respectively. The thermal properties of nanofluids and hybrid nanofluids are summarised in Table 1. The volume percentages of Al_2O_3 and Cu nanomaterials, respectively, are ϕ_1 and ϕ_2. The hybrid nanofluid is converted to a second-grade fluid by putting $\phi_1 = 0 = \phi_2$. Here, the liquid density ρ_{hnf}, dynamic viscosity μ_{hnf}, heat capacity $(\rho C)p_{hnf}$, electrical conductivity σ_{hnf}, and thermal conductivity of hybrid nanofluid k_{hnf}. For Al_2O_3 and Cu nanoparticles, the subscripts f, nf, hnf, s_1 and s_2 signify the fluid, nanofluid, hybrid nanofluid, and solid components, accordingly. Eq (9) also shows the physical characteristics of engine oil, Al_2O_3 nanoparticles, and Cu nanoparticles.

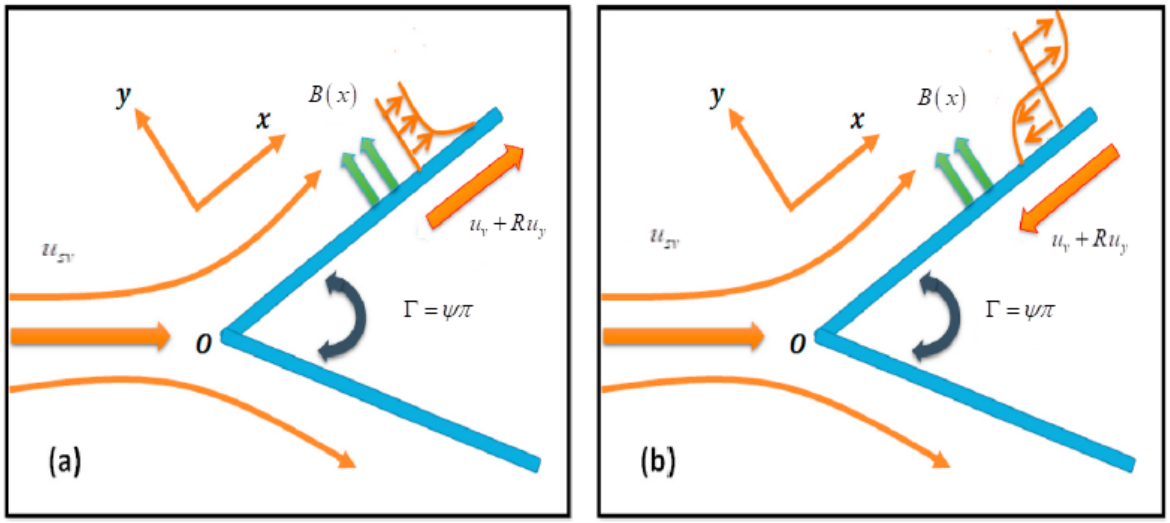

Figure 1. Flow figures (a) stretching Riga wedge and (b) shrinking Riga wedge.

Table 1. The Al_2O_3 thermo-physical properties along with Cu and EO [25].

Physical properties	$\rho\left(kg/m^3\right)$	$\rho c_p\left(J/kgK\right)$	$k\left(\mathrm{W}/mK\right)$	$\sigma\left(\Omega/m\right)^{-1}$
EO	884	1910	0.144	300
Al_2O_3	3970	765	40	3.69×10^7
Cu	8933	385	401	5.96×10^7

The following similarity transformations are illustrated for the governing Eqs (1)–(3) with the constraints (4) in a much simple way [36,50]. Where the stream function ω can be specified as $v=-\partial\omega/\partial x,$ and $u=\partial\omega/\partial y,$ while the similarity variable is η:

$$\left.\begin{aligned}&\omega=\sqrt{U_{sv}\nu_f}\,x^{(m+1)/2}f(\eta),\ \ \eta=\sqrt{\frac{U_{sv}}{\nu_f}}x^{(m-1)/2}y,\ \theta(\eta)=\frac{T-T_\infty}{T_w-T_\infty},\ u=U_{sv}x^m f'(\eta),\\&v=-\sqrt{U_{sv}\nu_f}\,x^{(m-1)/2}\left(\frac{m+1}{2}\right)\left(\frac{m-1}{m+1}\eta f'(\eta)+f(\eta)\right).\end{aligned}\right\}\tag{5}$$

Equations (2)–(4) may be reduced to a set of nonlinear ODEs in the setting of the above-mentioned relations by using the similarity transformations (5):

$$\begin{aligned}&\frac{\mu_r}{\rho_r}f'''+\left(\frac{2m}{m+1}\right)\left(-(f')^2+1\right)+\frac{\alpha}{\rho_r}\left((3m-1)ff'''+\left(\frac{3m-1}{2}\right)(f'')^2+(m-1)\eta f''f'''-\left(\frac{m+1}{2}\right)ff^{iv}\right)\\&+M_h\exp\left(-a_h\eta\right)+ff''=0,\end{aligned}\tag{6}$$

$$\begin{aligned}&\frac{k_r}{(\rho Cp)_r}\theta''+\frac{\mathrm{Nr}}{(\rho Cp)_r}\left(1+\theta(\theta_w-1)\right)^3\theta''+3\frac{\mathrm{Nr}}{(\rho Cp)_r}(\theta')^2(\theta_w-1)\left(1+\theta(\theta_w-1)\right)^2+\frac{2\,\mathrm{Pr}\,\theta H}{(\rho Cp)_r(m+1)}\\&+\mathrm{Pr}\,f\theta'=0,\end{aligned}\tag{7}$$

with boundary conditions are

$$\begin{aligned}&f(\eta)=0,\ f'(\eta)=S+\lambda\mu_r f''(\eta),\ k_r\theta'(\eta)=-B_i\left(1-\theta(\eta)\right),\ \text{ at }\ \eta\to0,\\&f'(\eta)=1,\ f''(\eta)=0,\ \theta(\eta)=0,\ \text{at }\ \eta\to\infty,\end{aligned}\tag{8}$$

where Modified Hartmann number $M_h=\pi j_0M_0/4u_{sv}^2$, second-grade fluid parameter $\alpha=2\alpha_1b/\mu_f$, the stretching/shrinking parameter $S=U_v/U_{sv}$, non-dimensional parameter $a_h=(\pi/d)\sqrt{2\nu_f/(m+1)},$ slip parameter $\lambda=R\mu_f\sqrt{U_{sv}/\nu_f}$, Prandtl number $\mathrm{Pr}=\alpha_f/\nu_f$, heat source parameter $H=Q_0/(\rho Cp)_f$, thermal radiation $Nr=-16\delta^*T_\infty^3a/3k^*k_f$, Biot number $B_i=\left(h_f/k_f\right)\sqrt{2x\nu_f/U_{sv}(m+1)},$ and temperature difference $\theta_r=T_f/T_\infty$ [6,11,12].

The thermophysical properties of the hybrid nanofluids are [11,25]:

$$\left.\begin{aligned}
&\mathrm{A}_2=\frac{\rho_{hnf}}{\rho_f}=\left[\left(1-\phi_2\right)\left\{\left(1-\phi_1\right)+\frac{\rho_{s_1}\phi_1}{\rho_f}\right\}+\frac{\rho_{s_2}\phi_2}{\rho_f}\right],\quad \mathrm{A}_1=\frac{\mu_{hnf}}{\mu_f}=\left(1-\phi_1\right)^{-2.5}\left(1-\phi_2\right)^{-2.5},\\
&\mathrm{A}_4=\frac{\left(\rho C_\rho\right)_{hnf}}{\left(\rho C_\rho\right)_f}=\frac{\phi_2\left(\rho C_\rho\right)_{s_2}}{\left(\rho C_\rho\right)_f}+\left(1-\phi_2\right)\left[\left(1-\phi_1\right)+\frac{\left(\rho C_\rho\right)_{s_1}\phi_1}{\left(\rho C_\rho\right)_f}\right],\\
&\mathrm{A}_3=\frac{k_{hnf}}{k_{nf}}=\frac{2k_{nf}-2\phi_1\left(k_{s_1}-k_{nf}\right)+k_{s_1}}{2k_{nf}+\phi_1\left(k_{s_1}-k_{nf}\right)+k_{s_1}},\quad \frac{k_{nf}}{k_f}=\frac{2k_f-2\phi_2\left(k_{s_2}-k_f\right)+k_{s_2}}{2k_f+\phi_2\left(k_{s_2}-k_f\right)+k_{s_2}}.
\end{aligned}\right\} \tag{9}$$

2.1. Physical interest

The quantities of physical interest are given by.
(i): The skin friction coefficient Cf_x and nusslt number Nu_x are defined by

$$Cf_x=\frac{1}{\rho_f u_e^2}\left[\mu_{hnf}\frac{\partial u}{\partial y}+\alpha_1\left\{u\frac{\partial^2 u}{\partial x\partial y}+v\frac{\partial^2 u}{\partial y^2}+2\frac{\partial u}{\partial y}\frac{\partial u}{\partial x}\right\}\right]_{y=0} \tag{10}$$

$$Nu_x=-\frac{x}{k_f\left(T_w-T_\infty\right)}\left[k_{hnf}\frac{\partial u}{\partial y}+\frac{16\sigma^* T_\infty^3}{3k^*}\frac{\partial u}{\partial y}\right]_{y=0}. \tag{11}$$

Then employ (5) into (10) and (11), yielding the following relationship:

$$\sqrt{\mathrm{Re}_x}Cf_x=\left(\mathrm{A}_1 f''(0)+\alpha_1\left(\begin{aligned}&mf'(0)f''(0)+\left(\frac{5m-1}{2}\right)f'(0)f''(0)\\&+(m-1)\eta f''(0)f''(0)+\left(\frac{m+1}{2}\right)f(0)f'''(0)\end{aligned}\right)\right), \tag{12}$$

$$\left(\mathrm{Re}_x\right)^{-0.5}Nu_x=-\left(\mathrm{A}_3+Nr\left(1+\theta(0)\left(\theta_w-1\right)\right)^3\right)\theta'(0), \tag{13}$$

where $Re_x=u_e x/\nu_f$ is the x-axis local Reynolds number.

2.2. Fuzzification

In practice, a change in the volume fraction value can impact the temperature and velocity profiles of a nanofluid and hybrid nanofluid. As a result, the nanoparticle volume fraction is viewed as a fuzzy parameter in terms of a TFN (see Table 2) to examine the current problem. The governing ODEs are converted into FDEs with help of σ-cut technique. Also, σ-cut range from 0 to 1 and controls the fuzziness of the TFN. For further information about this topic see the literature [59–70].

Let $\phi=\left[0,0.05,0.1\right]$ be a TFN defined entirely by three quantities: 0 (lower bound), 0.05 (most belief value), and 0.1 (upper bound) are shown in Figure 2. By the TFN, the Membership

function $M(\phi)$ can be expressed as:

$$M(\phi)=\begin{cases}\dfrac{0-\eta}{0.05-0} & \text{for} \quad \eta\in[0,\,0.05],\\ \dfrac{\eta-0.1}{0.1-0.05} & \text{for} \quad \eta\in[0.05,\,0.1],\\ 0, & \text{otherwise.}\end{cases} \tag{14}$$

TFNs are converted into interval numbers using σ-cut the approach, which is written as $\bar{\theta}(\eta,\sigma)=[\theta_1(\eta;\sigma),\theta_2(\eta;\sigma)]=[0+\sigma(0.05-0),\,0.1-\sigma(0.1-0.05)]$, where $0\le\sigma$-cut ≤ 1.

To handle such TFNs use FDEs with the help of the σ-cut technique. The FDEs are converted into lower $\theta_1(\eta;\sigma)$ and upper bounds $\theta_2(\eta;\sigma)$.

Table 2. In terms of TFN, the following parameters are detailed [25].

Fuzzy Numbers	Crisp value	TFN	σ-cut approach
$\phi_1\ (Al_2O_3)$	[0.01-0.04]	[0, 0.05, 0.1]	$[0.05\sigma,\,0.1-0.05\sigma],\ \sigma\in[0,1]$
$\phi_2\ (Cu)$	[0.01-0.04]	[0, 0.05, 0.1]	$[0.05\sigma,\,0.1-0.05\sigma],\ \sigma\in[0,1]$

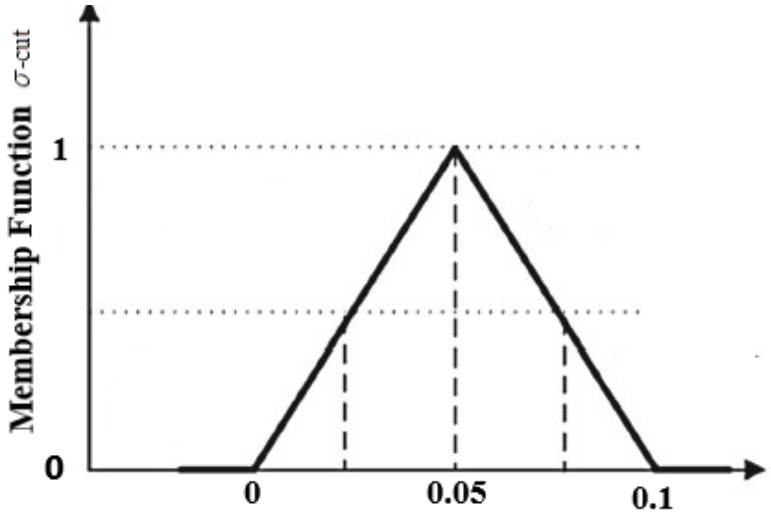

Figure 2. Membership function of TFN.

2.3. Numerical scheme

The differential type fluid model's governing flow equations are highly nonlinear, and exact solutions to the governing nonlinear problem are impossible to find due to the great complexity. In Fluid dynamics many problems are in non-linear form. The numerical techniques generally can be applied to nonlinear problems in the computation domain. This is an obvious advantage of numerical methods over analytic ones that often handle nonlinear problems in simple domains and it has taken less time to solve. bvp4c is a finite difference code that implements the three-stage Lobatto IIIa

formula. This is a collocation formula and the collocation polynomial provides a C1-continuous solution that is fourth-order accurate uniformly in the interval of integration. Mesh selection and error control are based on the residual of the continuous solution. Consequently, for these sorts of problems, a numerical methodology can be utilised to determine the numerical solution. By converting the present governing problem into an associated of first-order equations, we can achieve this. Here, we are discussing

$$f = G_1,\ f' = G_2,\ f'' = G_3,\ f''' = G_4,\ f'''' = G_4',\ \theta = G_5,\ \theta' = G_6, \tag{15}$$

$$G_4' = \frac{2\rho_r}{\alpha(m+1)G_1}\left[\begin{array}{l}\dfrac{\mu_r}{\rho_r}G_4 + \left(\dfrac{2m}{m+1}\right)\left(1-(G_2)^2\right)\\ +\dfrac{\alpha}{\rho_r}\left((3m-1)G_2G_3 + \left(\dfrac{3m-1}{2}\right){G_3}^2 + (m-1)\eta G_3G_4\right)\\ +M_h\exp(-a_h\eta) + G_1G_3\end{array}\right], \tag{16}$$

$$G_6' == \frac{-(\rho Cp)_r}{k_r + \left(1+G_5(\theta_w-1)\right)^3}\left[\begin{array}{l}\dfrac{3\,\mathrm{Nr}}{(\rho Cp)_r}(G_6)^2(\theta_w-1)\left(1+G_5(\theta_w-1)\right)^2 + \dfrac{\mathrm{Pr}\,G_5H}{(\rho Cp)_r}\\ +\mathrm{Pr}\,G_1G_6\end{array}\right], \tag{17}$$

with boundary conditions are

$$\begin{aligned} &G_1 = 0,\ G_2 = S + \lambda\mu_r G_3(\eta),\ k_r G_6(\eta) = -B_i\left(1-G_1(\eta)\right),\ \text{ at } \eta \to 0,\\ &G_2(\eta) = 1,\ G_3(\eta) = 0,\ G_5(\eta) = 0,\ \text{at } \eta \to \infty. \end{aligned} \tag{18}$$

The above set of ODEs (16) and (17) with BCs (18) can be numerically explained by employing the bvp4c technique in MATLAB, which is a finite-difference algorithm with the highest residual error of 10^{-6}.

3. Results and discussion

The concentration of the investigation is to establish the significance of fuzzy volume fraction, heat generation and nonlinear radiation, on the heat transport properties of second-grade hybrid $(Al_2O_3$+Cu/EO$)$ nanofluid flow over a shrinking/stretching Riga wedge. The bvp4c technique which builds in MATLAB is utilized to acquire the outcomes. The numerical results of flow rate, local Nusselt number, skin friction, and temperature were determined for various values of parameters $\mathrm{Pr} = 2.1,\ Nr = 0.7,\ M_h = 0.2,\ H = 0.1,\ \alpha = 0.7,\ m = 0.3,\ a_h = 0.3,\ \theta_r = 1.1,\ B_i = 0.8,$ $\lambda = 0.1,$ and $S = 0.6.$ Also, a comparison of second-grade fluid and hybrid nanofluid discussion in Figures 3–12.

A comparison table is also created to validate our computations with previous results, which is shown in Table 3. The present result is better as compared to the existing results.

Table 3. Comparisons of $-f''(0)$ with past published articles when $M_h = \alpha = \lambda = m = 0$.

Watanabe [28]	Kakar et al. [50]	Yacob et al. [29]	Present result
0.4696	0.4696	0.4696	0.4695

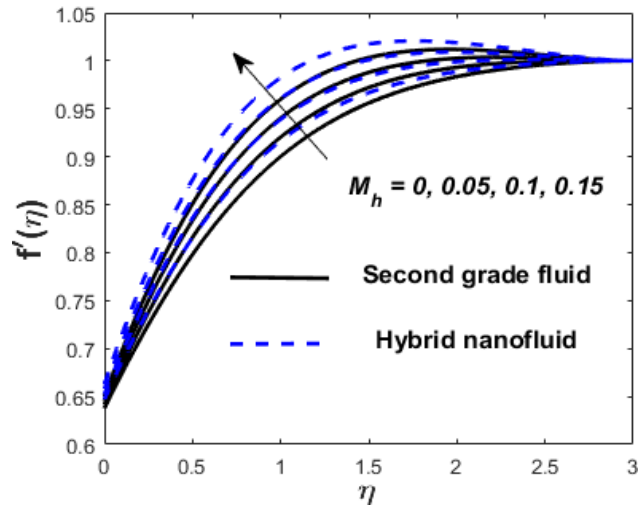

Figure 3. M_h against $f'(\eta)$.

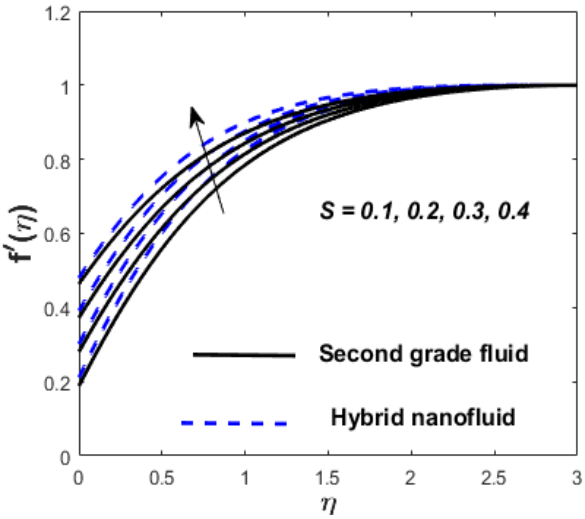

Figure 4. S against $f'(\eta)$.

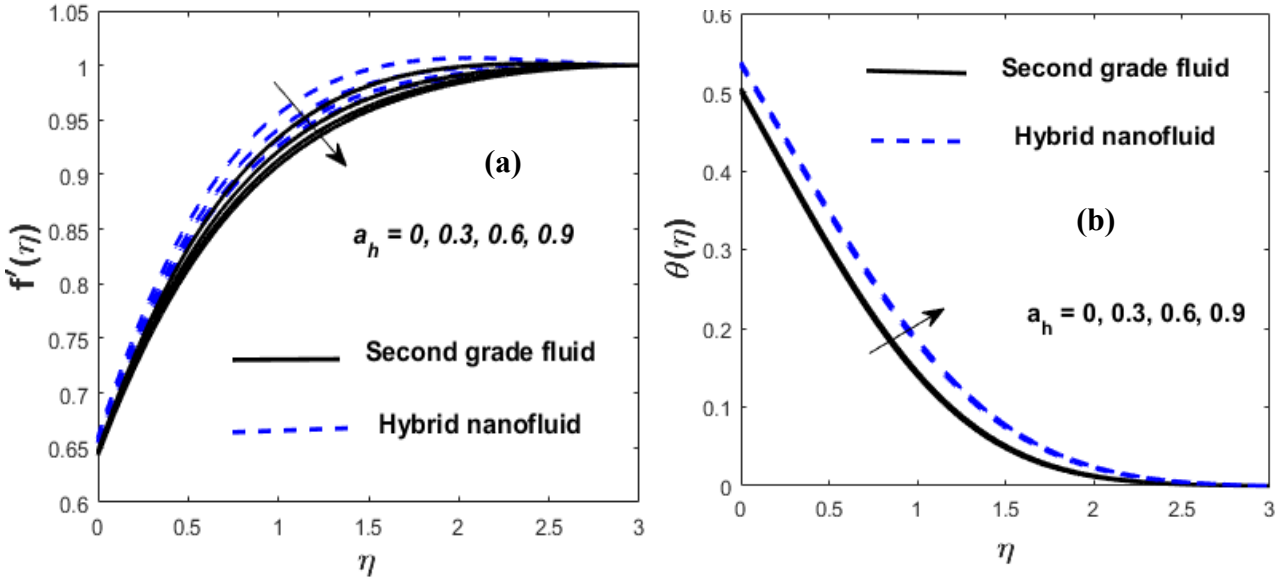

Figure 5. a_h against $f'(\eta)$ and $\theta(\eta)$.

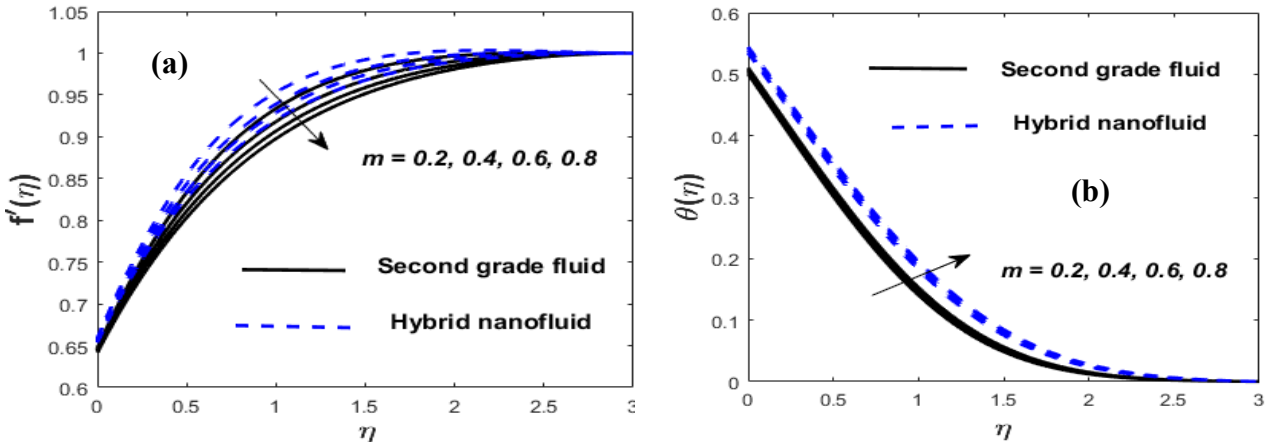

Figure 6. m against $f'(\eta)$ and $\theta(\eta)$.

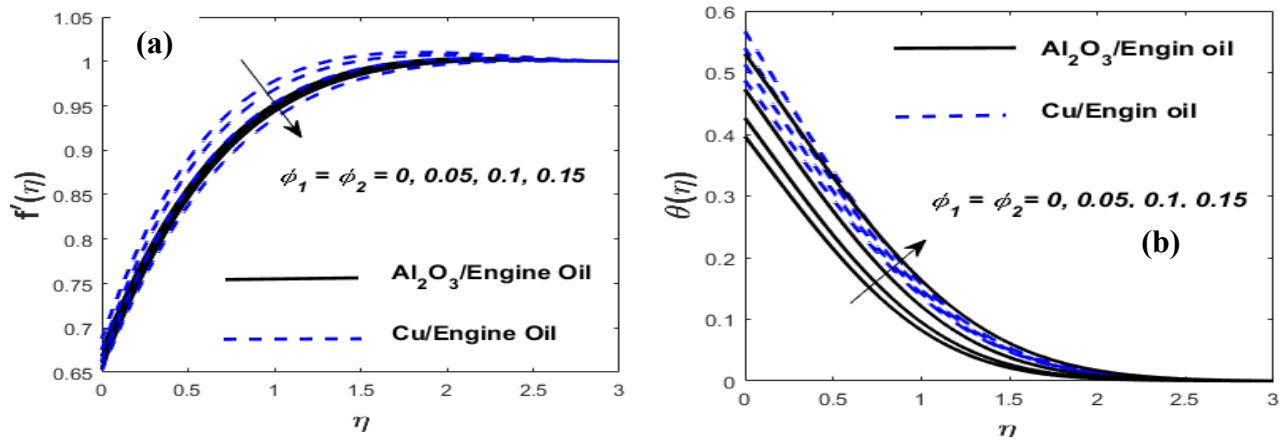

Figure 7. ϕ_1 and ϕ_2 against $f'(\eta)$ and $\theta(\eta)$.

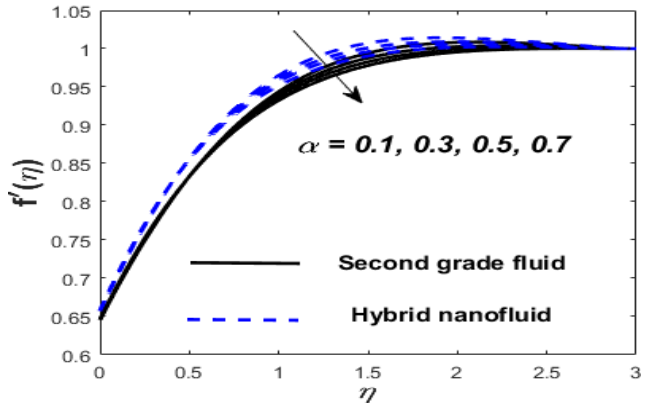

Figure 8. α against $f'(\eta)$.

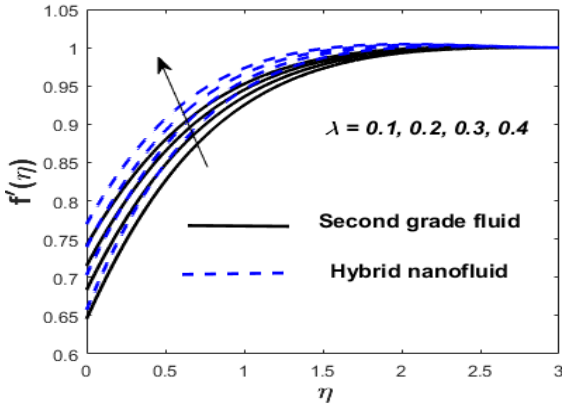

Figure 9. λ against $f'(\eta)$.

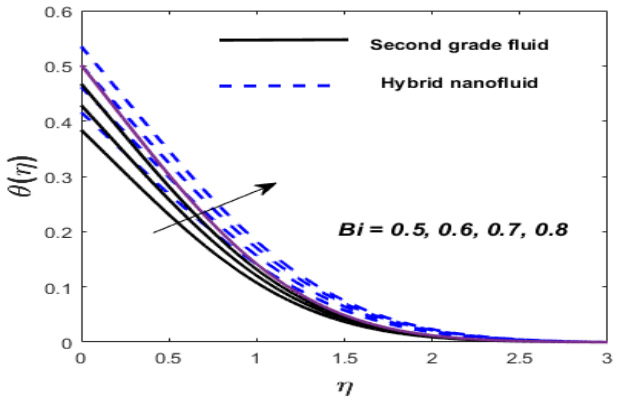

Figure 10. B_i against $\theta(\eta)$.

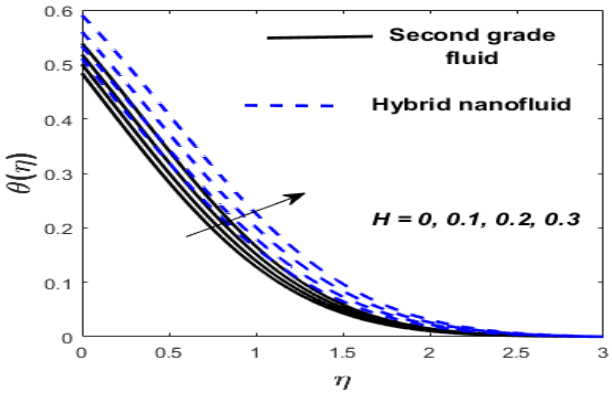

Figure 11. H against $\theta(\eta)$.

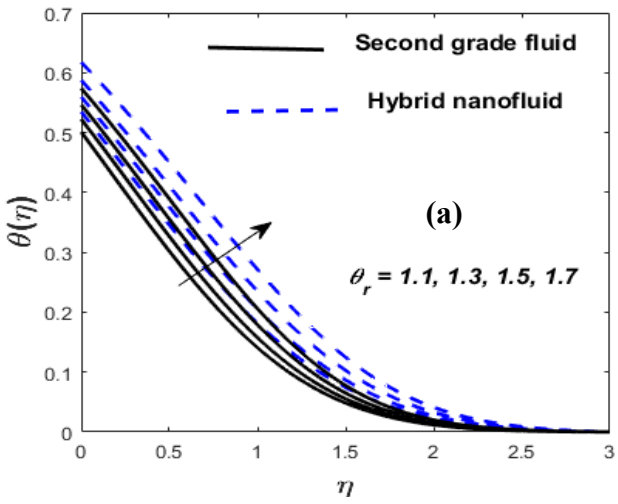

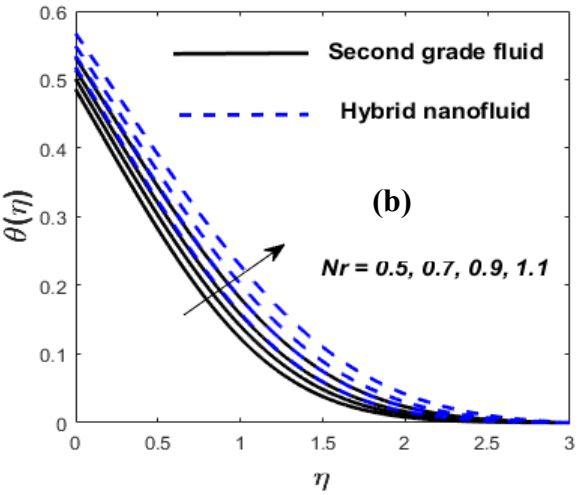

Figure 12. θ_r and Nr against $\theta(\eta)$.

Figure 3 exposes the influence of the modified Hartmann number (M_h) on the flow rate. It is perceived, that hybrid nanofluid velocity rises more rapidly than that of a second-grade fluid. The momentum boundary layers thin slightly as the M_h strength grows. Physically, a higher M_h determines the intensity of the external electric field, which promotes fluid flow and, consequently, Lorentz force produces. Figure 4 shows the velocity profile for varying values of the shrinking/stretching parameter (S). As the magnitude of S grows the fluid and hybrid nanofluid's flow rate upsurges. This is due to the uniform movement of the fluid velocity with the boundary surface. The momentum boundary layer thickens physically, causing the flow rate to rise. As a result, no force opposes the fluid's flow across the sheet's surface. The inspiration of the dimensionless parameter (a_h) on flow rate and temperature profiles is portrayed in Figure 5. With swelling a_h inputs, the velocity of both fluids decreases while the thermal efficiency improves. Lorentz forces cause the flow of fluid to decrease while the heat transfer rate improves when the a_h is raised. The velocity profile and temperature distribution for varying wedge angle parameter (m) are plotted in Figure 6. When m is larger, the velocity of the second-grade fluid and hybrid nanofluid declines

while the temperature of the second-grade fluid and hybrid nanofluid improves. Physically, the velocity declines due to boundary layer thickness improving whereas temperature raises. Figure 7 shows how the concentration of nanoparticles affects the flow and thermal fields of fluid and hybrid nanofluids. It has been noted that with the growth of ϕ_1 and ϕ_2, the velocity reduces whereas the thermal field is improved. Physically, the thermal and momentum boundary layers become denser for the higher volume fraction ϕ_1 $\left(Al_2O_3/EO\right)$ due to the presence of $\left(Al_2O_3+Cu/EO\right)$ hybrid nanoparticles in the ordinarily fluid, which generates too much resistance than fluid, and therefore, the velocity diminishes, and the heat of the fluid rises. The density of the hybrid nanofluid and fluid upsurges as the larger values of ϕ_2 $\left(Cu/EO\right)$, boost the heat and reduce velocity. As an outcome, the intermolecular interactions between the particles of hybrid nanofluids strengthen, and the hybrid nanofluid and fluid's heat transfer rate rise. The inspiration of the non-Newtonian parameter (α), on the velocity profile is shown in Figure 8. The velocity decreases meaningfully as the value of α is increased. This feature resulted in a significant rise in the thickness of the momentum boundary layer. The fact is that larger normal stress puts a push on the neighbouring particles, forcing them to move quickly. The velocity slip (λ) imprinted in Figure 9 represents the fluid flow. The velocity slip leads the velocity to grow, as has been shown. The velocity slip is predicted to cause additional disruption and accelerate the fluid motion. Physically, when velocity slip rises, the fluid velocity intensifies, resulting in higher applied forces to push the expanding wedge and energy transfer to the liquid. However, due to their importance in the thermophysical properties of hybrid nanofluid, it is noticed that hybrid nanofluid has the highest velocity when compared to fluid. Features of the Biot number (B_i) on the heat flux are reviewed in Figure 10. Larger B_i indicates that more heat is transported from the surface to the nanoparticles, and as a consequence, the temperature rises. Figure 11 indicates the impact of the heat source parameter (*H*) on the heat flux. It is recognized that as the *H* goes up, the heat flow enhances. Also, as compared to a second-grade fluid, the heat transmission rate of a hybrid nanofluid is higher. A considerable amount of heat energy is released from the wedge to the working fluid during the heat generation process, which strengthens the temperature field in the boundary layer region near the stretching/shirking wedge. Furthermore, at a smaller distance from the wedge, the temperature profile decays to zero. The influence of the temperature ratio (θ_r) and the radiation parameter (*Nr)* on the heat flux is demonstrated in Figure 12. It is evident that the temperature field upsurges when θ_r and *Nr* are raised. Physically, a larger θ_r indicates a significant temperature difference between the wedge wall and the surrounding environment. The boundary layer thickness improves as the temperature varies. Physically, the radiative component enhances small particle mobility, pushing random moving particles to collide and converting frictional energy to heat energy. A hybrid nanofluid's temperature is higher than that of a conventional fluid in both cases.

Impressions of various parameters $M_h, \phi_1, \lambda, \alpha, \phi_2$ and Pr on the local skin friction and Nusselt number are demonstrated in Figures 13–15. Variations of Cf_x, with M_h for several values of α are plotted in Figure 13. It is observed that when α is improved the skin-friction coefficient cultivates while M_h shows the opposite behaviour. Lorentz's effect raises the skin fraction on the Riga wedge's surface while reducing the distance away from it. Figure 14 exhibits Cf_x fluctuations with M_h for numerous λ values. The drag force declined when M_h and λ upsurged. The Nu_x lowers by way of ϕ_1 increase while heat transfer rate improved when ϕ_2 increasing as shown in

Figure 15. Physically, the heat emitted from the wedge surface when enhancing ϕ_1.

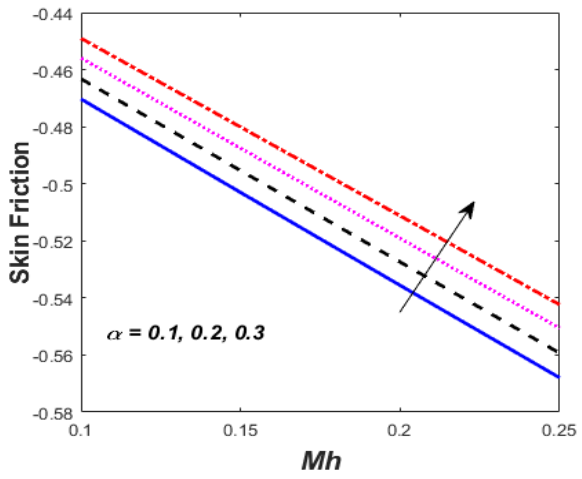

Figure 13. Impact of *Mh* and α on C_{fx}.

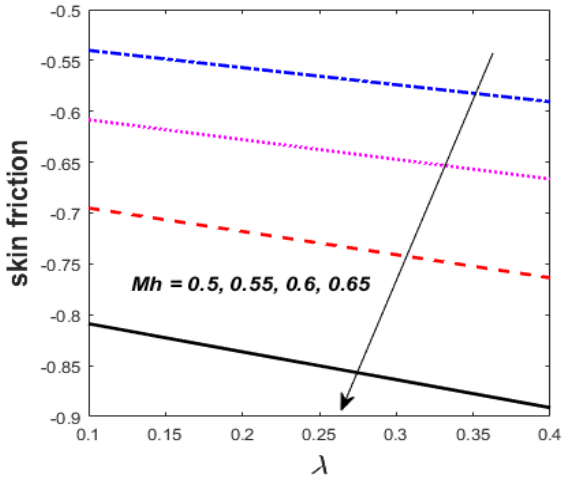

Figure 14. Impact of *Mh* and λ on C_{fx}.

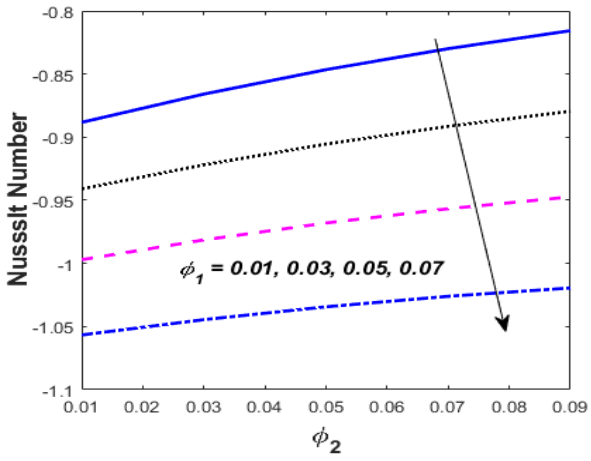

Figure 15. Impact of ϕ_1 and ϕ_2 on Nu_x.

The performance of various significantly flow parameters by the local coefficient of skin friction and Nusselt number is explored in Table 4. For larger values of M_h, m, ϕ_1, ϕ_2 and λ progress the skin friction whereas a_h, and α decrease the local skin friction factor. The nanoparticles are dragged when a perpendicular magnetic force is applied to a hybrid nanofluid moving across a Riga wedge, boosting the skin fraction. The outcome of the same engineering parameters on the Nusselt number is shown in the next column of Table 4. When the a_h, α, m, Nr, λ, and ϕ_1 are improved, then the heat transfer rate is boosted while it drops for the larger values of the Pr, M_h, and ϕ_2. The heat transmission rate of hybrid nanofluids is higher than the regular fluids.

Table 4. Numerical values of $-f''(0)$ and $\theta'(0)$ for different values of control parameters.

M_h	a_h	α	m	Nr	Pr	λ	ϕ_1	ϕ_2	$-f''(0)$	$\theta'(0)$
0.0									0.5072290	–0.956224
0.1									0.5764743	–0.948794
0.2									0.6404172	–0.941762
	0.2								0.5815562	–0.948020
	0.3								0.5764741	–0.948794
	0.4								0.5719610	–0.949469
		0.5							0.5859796	–0.946942
		0.6							0.5836635	–0.947490
		0.7							0.5815564	–0.948020
			0.1						0.3925970	–0.947044
			0.2						0.4889002	–0.946849
			0.3						0.5815564	–0.948020
				0.1					0.5799782	–0.580593
				0.2					0.5796537	–0.639745
				0.3					0.5796537	–0.699898
					1				0.5796537	–1.105734
					2				0.5796537	–0.959449
					3				0.5796537	–0.868373
						0.1			0.5796537	–0.948531
						0.2			0.5397714	–0.940017
						0.3			0.5033102	–0.933319
							0.01		0.4835550	–0.877424
							0.02		0.4934136	–0.904935
							0.03		0.5033102	–0.933319
								0.01	0.4684174	–0.956878
								0.02	0.4860501	–0.944530
								0.03	0.5033102	–0.933319

Figure 16 illustrate the fuzzy temperature profile $(\theta(\eta, \sigma))$ of Al_2O_3+Cu/EO by considering the volume fraction as a TFN, i.e., ϕ_1, and ϕ_2 = [0.0, 0.05, 0.1]. For triangular MFs, four sub-plots illustrate the fuzzy temperatures for varying values of η, such as 0.25, 0.5, 0.75, and 1. On the vertical axis is the MF of the fuzzy temperature profile for σ-cut$(0 \le \sigma\text{-cut} \le 1)$, while on the horizontal axis is $\theta(\eta, \sigma)$ for different values of η. The obtained fuzzy temperatures are TFN but not triangle-symmetric, while both fuzzy volume percentage is TFN and symmetric. The nonlinearity of the governing differential equation may cause these changes. Hybrid nanofluids were also shown to have a larger width than nanofluids. Consequently, the TFN considers the hybrid nanofluid to be uncertain. On the other way, Figure 16 demonstrates the comparison of nanofluids Al_2O_3/EO (ϕ_1), Cu/EO (ϕ_2), and Al_2O_3+Cu/EO hybrid nanofluids over MF for several values of η. We focus

on three possible outcomes in these graphics. The case when ϕ_1 is treated as TFN and $\phi_2 = 0$ is signified by purple dotted lines. The case when ϕ_2 is treated as TFN and $\phi_1 = 0$ is denoted by red dotted lines. The hybrid nanofluid with both ϕ_1 and ϕ_2 non-zero is shown in the third case by blue lines. It can be perceived that the hybrid nanofluid performs better due to the temperature variance in the hybrid nanofluid being more prominent than both nanofluids. Physically, The combined thermal conductivities of Al_2O_3 and Cu are added in a hybrid nanofluid to provide the maximum transfer of heat. When a comparison of Al_2O_3/EO and Cu/EO nanofluids is analyzed, Al_2O_3/EO has a higher heat transfer rate because Al_2O_3 has a higher thermal conductivity than Cu.

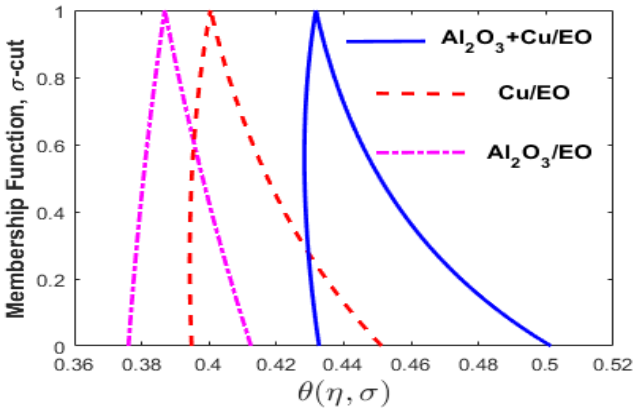

At η=0.25

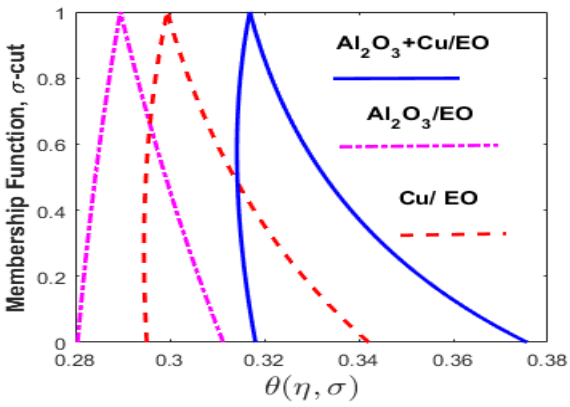

At η=0.5

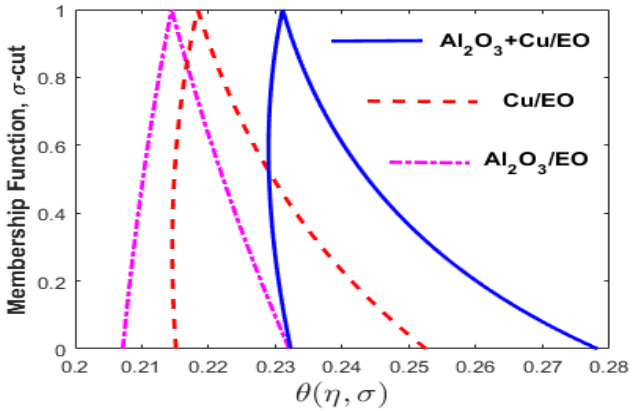

At η=0.75

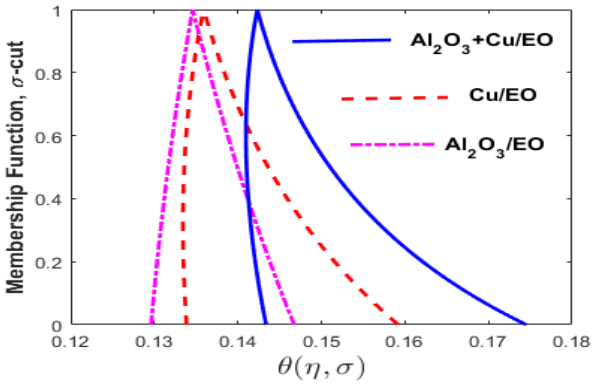

At η=1

Figure 16. Comparison of nanofluids Al_2O_3/EO, Cu/EO and Al_2O_3+Cu/EO hybrid nanofluids for various values of η.

4. Conclusions

A numerical investigation of second-grade hybrid (Al_2O_3+Cu/EO) nanofluid flow across a stretching/shrinking Riga wedge is discussed in this article. Fuzzy nanoparticle volume fraction,

convective, nonlinear thermal radiation, and slip boundary conditions are also studied. Using some appropriate transformations, the governing PDEs are turned into non-linear ODEs. In Matlab, a numerical method known as the bvp4c strategy is used to solve the problem. In addition, when compared to previous results in the literature, the new numerical results are outstanding. The major findings are as follows:

- Improvement of the size of nanomaterials in Engine oil can boost the rate of heat transfer. When compared to a conventional second-grade fluid, a hybrid nanofluid $\left(Al_2O_3+Cu/EO\right)$ is found to be a better thermal conductor.
- With higher a_h, m, α, ϕ_1 and ϕ_2 the hybrid nanofluid and second-grade fluid velocity decline.
- Both fluid velocities are intensified by boosting the credit of M_h, S, a_h, m and λ.
- Thermal efficiency is improved when Nr, θ_r, a_h, m, H and B_i are amplified.
- The Nusselt number is reduced with the upsurge in M_h, and Pr while swelling with the rise in the a_h, m, α, and λ.
- For fuzzy analysis through the triangular membership function, the width between lower $\left(\theta_1(\eta,\sigma)\right)$ and upper $\left(\theta_2(\eta,\sigma)\right)$ bounds of fuzzy temperature profiles of hybrid nanofluids is maximum so the fuzziness is maximum as compared to nanofluids.
- For fuzzy heat transfer analysis, the Al_2O_3+Cu/EO hybrid nanofluids are extremely proficient of boosting the heat transfer rate when compared to Al_2O_3/EO and Cu/EO nanofluids, as showed by triangular fuzzy membership functions. Also, the Cu/EO nanofluid is better than Al_2O_3/EO the nanofluid when they are compared.
- The behaviour of the drag force is improved with the heightening of M_h, m, λ, ϕ_1 and ϕ_2 whereas the reverse trend can be seen for the a_h, and α.

The findings of this study can be used to drive future progress in which the heating system's heat outcome is analyzed with non-Newtonian nanofluids or hybrid nanofluids of various kinds (i.e., Maxwell, Third-grade, Casson, Carreau, micropolar fluids, etc.).

Acknowledgement

The authors extend their appreciation to the Deanship of Scientific Research, University of Hafr Al Batin for funding this work through the research group project no. (0033-1443-S).

Competing interests

The authors declare no competing interests.

References

1. G. Rasool, T. Zhang, A. Shafiq, Second grade nanofluidic fow past a convectively heated vertical Riga plate, *Phys. Scr.,* **12** (2019), 125212. https://doi.org/10.1088/1402-4896/ab3990
2. T. Abbas, M. Ayub, M. M. Bhatti, M. M. Rashidi, M. E. Ali, Entropy generation on nanofuid fow through a horizontal Riga-plate, *Entropy,* **18** (2016), 223. https://doi.org/10.3390/e18060223

3. A. B. Tsinober, A. G. Shtern, Possibility of increasing the flow stability in a boundary layer using crossed electric and magnetic fields, *Magnetohydrodynamics,* **3** (1967), 103–105.
4. S. Abdal, I. Siddique, A. S. Alshomrani, F. Jarad, I. S. U. Din, S. Afzal, Significance of chemical reaction with activation energy for Riga wedge flow of tangent hyperbolic nanofluid in existence of heat source, *Case Stud. Therm. Eng.,* **28** (2021), 101542. https://doi.org/10.1016/j.csite.2021.101542
5. K. Gangadhar, M. A. Kumari, A. J. Chamkha, EMHD flow of radiative second-grade nanofluid over a Riga plate due to convective heating: Revised Buongiorno's nanofluid model, *Arab. J. Sci. Eng.*, 2021, 1–11. https://doi.org/10.1007/s13369-021-06092-7
6. M. I. Khan, F. Alzahrani, Dynamics of viscoelastic fluid conveying nanoparticles over a wedge when bioconvection and melting process are significant, *Int. Commun. Heat Mass*, **128** (2021), 105604. https://doi.org/10.1016/j.icheatmasstransfer.2021.105604
7. D. Vieru, I. Siddique, M. Kamran, C. Fetecau, Energetic balance for the flow of a second-grade fluid due to a plate subject to shear stress, *Comput. Math. Appl.*, **4** (2008), 1128–1137. https://doi.org/10.1016/j.camwa.2008.02.013
8. A. Mahmood, C. Fetecau, I. Siddique, Exact solutions for some unsteady flows of generalized second grade fluids in cylindrical domains, *J. Prim. Res. Math.*, **4** (2008), 171–180. Available from: http://www.sms.edu.pk/jprm/media/pdf/jprm/volume_04/jprm10_4.pdf
9. M. Ramzan, M. Bilal, Time-dependent MHD nano-second grade fluid flow induced by a permeable vertical sheet with mixed convection and thermal radiation, *PLoS One*, **10** (2015). https://doi.org/10.1371/journal.pone.0124929
10. M. Ramzan, M. Bilal, U. Farooq, J. D. Chung, Mixed convective radiative flow of second grade nanofluid with convective boundary conditions: an optimal solution, *Res. Phys*., **6** (2016), 796–804. https://doi.org/10.1016/j.rinp.2016.10.011
11. S. K. Rawat, H. Upreti, M. Kumar, Comparative study of mixed convective MHD Cu-water nanofluid flow over a cone and wedge using modified Buongiorno's model in presence of thermal radiation and chemical reaction via Cattaneo-Christov double diffusion model, *J. Appl. Comput. Mech.,* 2020. Available from: https://jacm.scu.ac.ir/article_15395_9ede39b5e33cc127967e197282afed32.
12. S. Rajput, A. K. Verma, K. Bhattacharyya, A. J. Chamkha, Unsteady nonlinear mixed convective flow of nanofluid over a wedge: Buongiorno model, *Waves Random Complex*, 2021, 1–15. https://doi.org/10.1080/17455030.2021.1987586
13. A. Mishra, M. Kumar, Numerical analysis of MHD nanofluid flow over a wedge, including effects of viscous dissipation and heat generation/absorption, using Buongiorno model, *Heat Transfer*, **8** (2021), 8453–8474. https://doi.org/10.1002/htj.22284
14. R. Garia, S. K. Rawat, M. Kumar, M. Yaseen, Hybrid nanofluid flow over two different geometries with Cattaneo-Christov heat flux model and heat generation: A model with correlation coefficient and probable error, *Chinese J. Phys.*, **74** (2021), 421–439. https://doi.org/10.1016/j.cjph.2021.10.030
15. I. Siddique, M. Nadeem, J. Awrejcewicz, W. Pawłowski, Soret and Dufour effects on unsteady MHD second-grade nanofluid flow across an exponentially stretching surface, *Sci Rep.,* **12** (2022), 11811. https://www.nature.com/articles/s41598-022-16173-8
16. S. U. Choi, J. A. Eastman, Enhancing thermal conductivity of fluids with nanoparticles (No. ANL/MSD/CP-84938; CONF-951135-29), *Argonne National Lab.,* IL (United States), 1995. Available from: https://ecotert.com/pdf/196525_From_unt-edu.pdf

17. S. Suresh, K. P. Venkitaraj, P. Selvakumar, Effect of Al_2O_3-Cu/water hybrid nanofluid in heat transfer, *Exp. Therm. Fluid Sci.*, **38** (2012), 54–60. https://doi.org/10.1016/j.expthermflusci.2011.11.007
18. L. S. Sundar, A. C. Sousa, M. K. Singh, Heat transfer enhancement of low volume concentration of carbon nanotube-Fe_3O_4/water hybrid nanofluids in a tube with twisted tape inserts under turbulent flow, *J. Therm. Sci. Eng. Appl.*, **7** (2015), 021015. https://doi.org/10.1115/1.4029622
19. S. Nadeem, N. Abbas, A. U. Khan, Characteristics of three dimensional stagnation point flow of Hybrid nanofluid past a circular cylinder, *Results Phys.*, **8** (2018), 829–835. https://doi.org/10.1016/j.rinp.2018.01.024
20. S. Nadeem, N. Abbas, On both MHD and slip effect in micropolar hybrid nanofluid past a circular cylinder under stagnation point region, *Can. J. Phys.*, **97** (2018), 392–399. https://doi.org/10.1139/cjp-2018-017
21. S. Yan, D. Toghraie, L. A. Abdulkareem, A. Alizadeh, P. Barnoon, M. Afrand, The rheological behavior of MWCNTs-ZnO/water-ethylene glycol hybrid non-Newtonian nanofluid by using of an experimental investigation, *J. Mater. Res. Technol*., **9** (2020), 8401–8406. https://doi.org/10.1016/j.jmrt.2020.05.018
22. A. U. Rehman, R. Mehmood, S. Nadeem, N. S. Akbar, S. S. Motsa, Effects of single and multi-walled carbon nano tubes on water and engine oil based rotating fluids with internal heating, *Adv. Powder Technol*., **28** (2017), 1991–2002. https://doi.org/10.1016/j.apt.2017.03.017
23. N. A. L. Aladdin, N. Bachok, I. Pop, Cu-Al_2O_3/water hybrid nanofluid flow over a permeable moving surface in presence of hydromagnetic and suction effects, *Alex. Eng. J.,* **59** (2020), 657–666. https://doi.org/10.1016/j.aej.2020.01.028
24. N. S. Anuar, N. Bachok, N. M. Arifin, H. Rosali, Analysis of Al_2O_3-Cu nanofluid flow behaviour over a permeable moving wedge with convective surface boundary conditions, *J. King Saud Univ. Sci.,* **33** (2021), 101370. https://doi.org/10.1016/j.jksus.2021.101370
25. M. Nadeem, I. Siddique, J. Awrejcewicz, M. Bilal, Numerical analysis of a second-grade fuzzy hybrid nanofluid flow and heat transfer over a permeable stretching/shrinking sheet, *Sci. Rep.-UK,* **12** (2022), 1–17. https://www.nature.com/articles/s41598-022-05393-7
26. N. Joshi, A. K. Pandey, H. Upreti, M. Kumar, Mixed convection flow of magnetic hybrid nanofluid over a bidirectional porous surface with internal heat generation and a higher-order chemical reaction, *Heat Transfer*, **50** (2021), 3661–3682. https://doi.org/10.1002/htj.22046
27. N. Joshi, H. Upreti, A. K. Pandey, M. Kumar, Heat and mass transfer assessment of magnetic hybrid nanofluid flow via bidirectional porous surface with volumetric heat generation, *Int. J. Appl. Comput. Math.*, **7** (2021), 1–17. Available from: https://link.springer.com/article/10.1007/s40819-021-00999-3
28. T. Watanabe, Thermal boundary layers over a wedge with uniform suction or injection in forced flow, *Acta Mech.,* **83** (1990), 119–126. Available from: https://link.springer.com/article/10.1007/BF01172973
29. N. A. Yacob, A. Ishak, I. Pop, Falkner-Skan problem for a static or moving wedge in nanofluids, *Int. J. Therm. Sci*., **50** (2011), 133–139. https://doi.org/10.1016/j.ijthermalsci.2010.10.008
30. H. Upreti, A. K. Pandey, M. Kumar, Assessment of entropy generation and heat transfer in three-dimensional hybrid nanofluids flow due to convective surface and base fluids, *J. Porous Media*, **24** (2021). https://doi.org/10.1615/JPorMedia.2021036038

31. A. Mishra, M. Kumar, Velocity and thermal slip effects on MHD nanofluid flow past a stretching cylinder with viscous dissipation and Joule heating, *SN Appl. Sci.*, **2** (2020), 1–13. Available from: https://link.springer.com/article/10.1007/s42452-020-3156-7.
32. A. Mishra, H. Upreti, A comparative study of Ag-MgO/water and Fe3O4-CoFe2O4/EG-water hybrid nanofluid flow over a curved surface with chemical reaction using Buongiorno model, *Partial Differ. Eq. Appl. Math.*, **5** (2022), 100322, 2666–8181. https://doi.org/10.1016/j.padiff.2022.100322
33. M. Yaseen, S. K. Rawat, M. Kumar, Cattaneo-Christov heat flux model in Darcy-Forchheimer radiative flow of MoS2-SiO2/kerosene oil between two parallel rotating disks, *J. Therm. Anal. Calorim.*, 2022, 1–23. Available from: https://link.springer.com/article/10.1007/s10973-022-11248-0.
34. S. K. Rawat, M. Kumar, Cattaneo-Christov heat flux model in flow of copper water nanofluid through a stretching/shrinking sheet on stagnation point in presence of heat generation/absorption and activation energy, *Int. J. Appl. Comput. Math.*, **6** (2020), 1–26. Available from: https://link.springer.com/article/10.1007/s40819-020-00865-8.
35. A. Gailitis, O. Lielausis, On possibility to reduce the hydrodynamics resistance of a plate in an electrolyte, *Appl. Magn. Rep. Phys. Inst. Riga*, **12** (1961), 143–146. Available from: https://scirp.org/reference/ReferencesPapers.aspx?ReferenceID=1927365.
36. H. T. Basha, R. Sivaraj, I. L. Animasaun, Stability analysis on Ag-MgO/water hybrid nanofluid flow over an extending/contracting Riga wedge and stagnation point, *CTS*, **12** (2020), 6. https://doi.org/10.1615/ComputThermalScien.2020034373
37. G. Rasool, A. Wakif, Numerical spectral examination of EMHD mixed convection flow of second-grade nanofluid towards a vertical Riga plate used an advanced version of the revised Buongiorno's nanofluid model, *J. Therm. Anal. Calorim.,* **143** (2021), 2379–2393. Available from: https://link.springer.com/article/10.1007/s10973-020-09865-8.
38. G. K. Ramesh, G. S. Roopa, B. J. Gireesha, S. A. Shehzad, F. M. Abbasi, An electro-magneto-hydrodynamic flow Maxwell nanoliquid past a Riga plate: A numerical study, *J. Brazilian Soc. Mech. Sci. Eng.,* **39** (2017), 4547–4554. Available from: https://link.springer.com/article/10.1007/s40430-017-0900-z.
39. A. Shafiq, I. Zari, I. Khan, T. S. Khan, A. H. Seikh, E. S. M. Sherif, Marangoni driven boundary layer flow of carbon nanotubes toward a Riga plate, *Front. Phys.,* **7** (2020), 1–11. https://doi.org/10.3389/fphy.2019.00215
40. N. Ahmed, Adnan, U. Khan, S. T. Mohyud-Din, Influence of thermal radiation and viscous dissipation on squeezed flow of water between Riga plates saturated with carbon nanotubes, *Colloid. Surface. A.,* **522** (2017), 389–398. https://doi.org/10.1016/j.colsurfa.2017.02.083
41. M. Ayub, T. Abbas, M. M. Bhatti, Inspiration of slip effects on EMHD nanofluid flow through a horizontal Riga plate, *Eur. Phys. J. Plus*, **131** (2016), 1–9. https://doi.org/10.1140/epjp/i2016-16193-4
42. A. Zaib, R. U. Haq, A. J. Chamkha, M. M. Rashidi, Impact of partial slip on mixed convective flow towards a Riga plate comprising micropolar TiO2-kerosene/water nanoparticles, *Int. J. Numer. Meth. H.,* **29** (2018), 1647–1662. https://doi.org/10.1108/HFF-06-2018-0258
43. T. Abbas, M. Ayub, M. M. Bhatti, M. M. Rashidi, M. E. S. Ali, Entropy generation on nanofluid flow through a horizontal Riga plate, *Entropy*, **18** (2016), 223. https://doi.org/10.3390/e18060223

44. M. M. Bhatti, T. Abbas, M. M. Rashidi, Effects of thermal radiation and electro magneto hydrodynamics on viscous nanofluid through a Riga plate, *Multidiscip. Model. Ma.*, **12** (2016), 605–618. https://doi.org/10.1108/MMMS-07-2016-0029
45. E. Magyari, A. Pantokratoras, Aiding and opposing mixed convection flows over the Riga-plate, *Commun. Nonlinear Sci. Numer. Simul.*, **16** (2011), 3158–3167. https://doi.org/10.1016/j.cnsns.2010.12.003
46. J. Pang, K. S. Choi, Turbulent drag reduction by Lorentz force oscillation, *Phys. Fluids,* **16** (2004). https://doi.org/10.1063/1.1689711
47. Y. Liu, Y. Jian, W. Tan, Entropy generation of electromagnetohydrodynamic (EMHD) flow in a curved rectangular microchannel, *Int. J. Heat Mass Transf.,* **127** (2018), 901–913. https://doi.org/10.1016/j.ijheatmasstransfer.2018.06.147
48. N. A. Zainal, R. Nazar, K. Naganthran, I. Pop, Unsteady EMHD stagnation point flow over a stretching/shrinking sheet in a hybrid Al2O3-Cu/H2O nanofluid, *Int. Commun. Heat Mass,* **123** (2021), 105205. https://doi.org/10.1016/j.icheatmasstransfer.2021.105205
49. M. Bilal, Micropolar flow of EMHD nanofluid with nonlinear thermal radiation and slip effects, *Alex. Eng. J.*, **59** (2020), 965–976. https://doi.org/10.1016/j.aej.2020.03.023
50. N. Kakar, A. Khalid, A. S. Al-Johani, N. Alshammari, I. Khan, Melting heat transfer of a magnetized water-based hybrid nanofluid flow past over a stretching/shrinking wedge, *Case Stud. Therm. Eng.*, **30** (2022), 101674. https://doi.org/10.1016/j.csite.2021.101674
51. T. Abbas, T. Hayat, M. Ayub, M. M. Bhatti, A. Alsaedi, Electromagnetohydrodynamic nanofluid flow past a porous Riga plate containing gyrotactic microorganism, *Neural Comput. Appl.*, **31** (2019), 1905–1913. Available from: https://link.springer.com/article/10.1007/s00521-017-3165-7.
52. N. Joshi, H. Upreti, A. K. Pandey, MHD Darcy-Forchheimer Cu-Ag/H2O-C2H6O2 hybrid nanofluid flow via a porous stretching sheet with suction/blowing and viscous dissipation, *Int. J. Comput. Meth. Eng. Sci. Mech.*, 2022, 1–9. https://doi.org/10.1080/15502287.2022.2030426
53. A. Mishra, H. Upreti, A comparative study of Ag-MgO/water and Fe_3O_4-$CoFe_2O_4$/EG-water hybrid nanofluid flow over a curved surface with chemical reaction using Buongiorno model, *Partial Differ. Eq. Appl. Math.*, **5** (2022), 100322. https://doi.org/10.1016/j.padiff.2022.100322
54. S. Abdal, U. Habib, I. Siddique, A. Akgül, B. Ali, Attribution of multi-slips and bioconvection for micropolar nanofluids transpiration through porous medium over an extending sheet with PST and PHF conditions, *Int. J. Appl. Comput. Math.*, **7** (2021), 1–21. Available from: https://link.springer.com/article/10.1007/s40819-021-01137-9.
55. S. Abdal, I. Siddique, D. Alrowaili, Q. Al-Mdallal, S. Hussain, Exploring the magnetohydrodynamic stretched flow of Williamson Maxwell nanofluid through porous matrix over a permeated sheet with bioconvection and activation energy, *Sci. Rep.,* **12** (2022), 1–12. Available from: https://www.nature.com/articles/s41598-021-04581-1.
56. L. A. Zadeh, Fuzzy sets, *Inform. Control,* **8** (1965), 338–353. https://doi.org/10.1142/9789814261302_0021
57. S. Chang, L. Zadeh, On fuzzy mapping and control, *IEEE T. Syst. Man Cy.*, **2** (1972), 30–34. https://doi.org/10.1109/TSMC.1972.5408553
58. D. Dubois, H. Prade, Towards fuzzy differential calculus: part 3, differentiation, *Fuzzy Set. Syst.*, **8** (1982), 30–34. https://doi.org/10.1016/S0165-0114(82)80001-8
59. O. Kaleva, Fuzzy differential equations, *Fuzzy Set. Syst.*, **24** (1987), 301–307. https://doi.org/10.1016/0165-0114(87)90029-7

60. O. Kaleva, The cauchy problem for fuzzy differential equations, *Fuzzy Set. Syst.*, **24** (1990), 389–396. https://doi.org/10.1016/0165-0114(90)90010-4
61. S. Seikkala, On the fuzzy initial value problem, *Fuzzy Set. Syst.*, **24** (1987), 319–330. https://doi.org/10.1016/0165-0114(87)90030-3
62. G. Borah, P. Dutta, G. C. Hazarika, Numerical study on second-grade fluid flow problems using analysis of fractional derivatives under fuzzy environment, *Soft Comput. Tech. Appl. Adv. Intell. Syst. Comput.* 1248 (2021). https://doi.org/10.1007/978-981-15-7394-1_4
63. A. Barhoi, G. C. Hazarika, P. Dutta, Numerical solution of MHD Viscous flow over a shrinking sheet with second order slip under fuzzy environment, *Adv. Math. Sci. J.*, **9** (2020), 10621–10631. https://doi.org/10.37418/amsj.9.12.47
64. U. Biswal, S. Chakraverty, B. K. Ojha, Natural convection of nanofluid flow between two vertical flat plates with imprecise parameter, *Coupled Syst. Mech.,* **9** (2020), 219–235. https://doi.org/10.12989/csm.2020.9.3.219
65. M. Nadeem, A. Elmoasry, I. Siddique, F. Jarad, R. M. Zulqarnain, J. Alebraheem, N. S. Elazab, Study of triangular fuzzy hybrid nanofluids on the natural convection flow and heat transfer between two vertical plates, *Comput. Intell. Neurosc.,* **2021** (2021). https://doi.org/10.1155/2021/3678335
66. I. Siddique, R. M. Zulqarnain, M. Nadeem, F. Jarad, Numerical simulation of MHD Couette flow of a fuzzy nanofluid through an inclined channel with thermal radiation effect, *Comput. Intell. Neurosc.*, **2021** (2021), 1–16. https://doi.org/10.1155/2021/6608684
67. S. Chakraverty, S. Tapaswini, D. Behera, *Fuzzy differential equations and applications for engineers and scientists*, CRC Press, Boca Raton, 2016. https://doi.org/10.1201/9781315372853
68. M. Nadeem, I. Siddique, R. Ali, N. Alshammari, R. N. Jamil, N. Hamadneh, M. Andualem, Study of third-grade fluid under the fuzzy environment with Couette and Poiseuille flows, *Math. Probl. Eng.*, **2022** (2022). https://doi.org/10.1155/2022/2458253
69. I. Siddique, R. M. Zulqarnain, M. Nadeem, F. Jarad, Numerical simulation of mhd couette flow of a fuzzy nanofluid through an inclined channel with thermal radiation effect, *Comput. Intell. Neurosc.*, **2021** (2021). https://doi.org/10.1155/2021/6608684
70. M. Nadeem, I. Siddique, F. Jarad, R. N. Jamil, Numerical study of MHD third-grade fluid flow through an inclined channel with ohmic heating under fuzzy environment, *Math. Probl. Eng.*, **2021** (2021). https://doi.org/10.1155/2021/9137479
71. M. Bilal, H. Tariq, Y. Urva, I. Siddique, S. Shah, T. Sajid, et al., A novel nonlinear diffusion model of magneto-micropolar fluid comprising Joule heating and velocity slip effects, *Wave. Random Complex*, 2022, 1–17. https://doi.org/10.1080/17455030.2022.2079761
72. I. Siddique, R. N. Jamil, M. Nadeem, H. A. El-Wahed Khalifa, F. Alotaibi, I. Khan, et al., Fuzzy analysis for thin-film flow of a third-grade fluid down an inclined plane, *Math. Probl. Eng.*, **2022** (2022), 3495228. https://doi.org/10.1155/2022/3495228
73. I. Siddique, M. Nadeem, I. Khan, R. N. Jamil, M. A. Shamseldin, A. Akgül, Analysis of fuzzified boundary value problems for MHD Couette and Poiseuille flow, *Sci. Rep.-UK*, **12** (2022), 1–28. Available from: https://www.nature.com/articles/s41598-022-12110-x.